inter.noise
HAMBURG 2016

Tutorial on the Vibroacoustics of Composite Sandwich Panels

Stephen A. Hambric

Hambric Acoustics, LLC, www.hambricacoustics.com, hambricacoustics@gmail.com

ABSTRACT

Composite sandwich panels are used throughout the aerospace industry as lightweight, stiff structural components. While the vibroacoustic behavior of simple isotropic homogeneous panels are described in many textbooks and articles, the properties of composite sandwich panels are not as well documented. This tutorial describes basic analytic methods for estimating sandwich panel wavespeeds, modal frequencies, mobilities/conductances, and radiation resistances. Measured and simulated data from two example sandwich panels – a launch vehicle panel with free boundaries and a framed rotorcraft roof panel with simply supported boundary conditions - are shown to illustrate these concepts. Modal wavenumber analysis confirms the wavespeed estimating procedures. Mobility/conductance becomes dominated by shear waves at fairly low frequencies. Finally, the strong contribution of radiation damping to overall modal damping is evident in measured data.

Keywords: Vibroacoustics, composite sandwich panels
I-INCE Classification of Subjects Number(s): 42, 75
(See . http://www.inceusa.org/links/Subj%20Class%20-%20Formatted.pdf .)

1. INTRODUCTION

This paper continues a tutorial series on vibroacoustics I began with two articles in *Acoustics Today* magazine [1,2], and continued last year with a tutorial on sound transmission loss at *Internoise 2015* [3]. Over the past seven years my colleagues and I have worked on two large projects involving sandwich panels – honeycomb cores sandwiched between outer face sheets [4-10]. These panels are used extensively in the aerospace industry due to their high stiffness to mass ratios. These high ratios speed up flexural waves, leading to increased coupling between the panels and the surrounding air. Sandwich panel flexural waves also transition to pure shear waves at lower frequencies than in homogeneous panels, leading to higher mobilities.

The vibroacoustic behavior of flat rectangular isotropic homogeneous panels is well understood, and has been documented in many papers and textbooks. The vibration and sound radiation of sandwich panels is less well documented, motivating this tutorial. Using some of the general vibroacoustic quantities and methods outlined in [11-13] and drawing examples from previous Internoise articles [4-10], I explain flexural wavespeeds and modes of vibration, flexural mobilities, and radiation resistance of sandwich panels.

Two sandwich panels are shown in Figure 1. The top panel in the figure is representative of panels used on launch vehicles, is designed for high strength, and was tested with free boundary conditions. The bottom panel is representative of those used on rotorcraft roof panels, and is supported between a frame of beams (which is actually a mount for a rotorcraft transmission) which are similar to idealized analytic simple supports. Since the frame supports most of the rotorcraft loads, the roof panel is not as strong as the launch vehicle panel. The two panels provide a wide range of size, strength, and boundary conditions for this tutorial.

[1] hambricacoustics@gmail.com

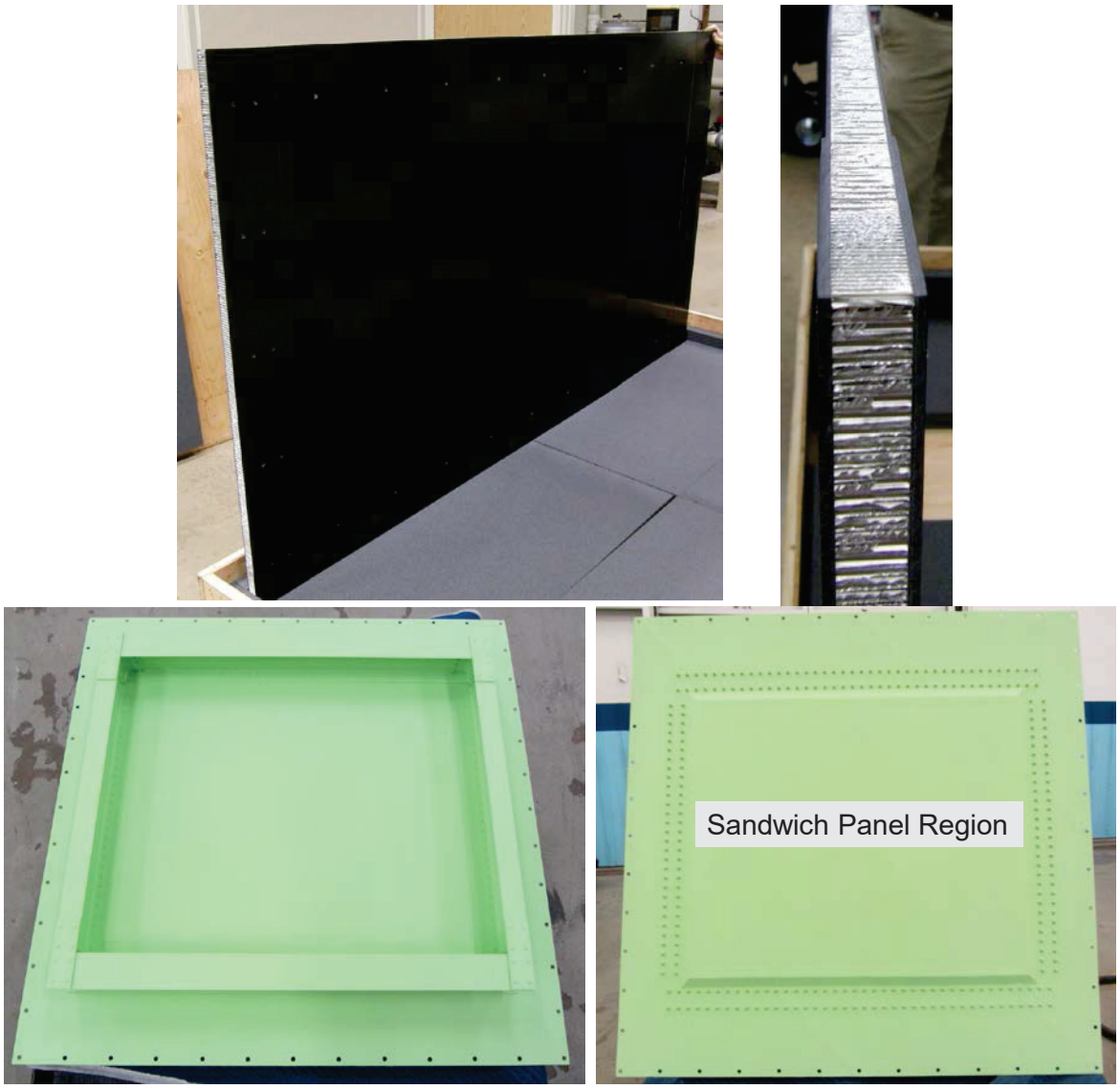

Figure 1. Launch vehicle panel (top) with free boundary conditions, and rotorcraft roof panel (bottom) simply supported between a frame structure.

2. FLEXURAL WAVESPEEDS AND MODES

2.1 Construction

Figure 2 shows a cross section of a sandwich panel. The upper and lower face sheets, typically made of aluminum or composite laminae, provide the flexural stiffness, and are assumed to have the same thickness (so the panel is symmetric about its neutral axis). Offsetting these sheets from the neutral axis increases stiffness by the 2nd power of the offset distance, thanks to the parallel axis theorem for area moment of inertia. A lightweight core is placed between the sheets to offset them, leading to extremely stiff, lightweight structures. The sheets are bonded to the core with an adhesive, (usually stiff enough so that its effects may be ignored).

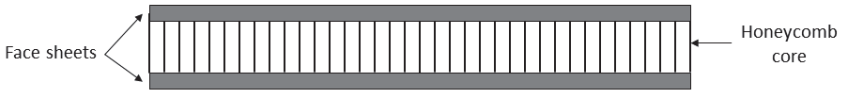

Figure 2. A typical sandwich panel cross section.

While the face sheets provide the flexural rigidity in a sandwich panel (proportional to the in-plane extensional elastic moduli), the cores provide transverse shear stiffness. There are many core types used in sandwich panels. The simplest are stiff foams, with castable materials embedded with air voids. Other cores are corrugated, resembling arrays of 'S' patterns, like cardboard. Perhaps the most popular cores are honeycomb cell patterns, as shown in Figure 3. Cores are made from metal, or nonmetallic materials. Nomex, which is a stiffened paper, is quite popular, along with Aramid and Kevlar. Most cores are made of stacked corrugated sheets. When assembled, the honeycomb cells are clearly visible. However, the shear stiffnesses of the core are different for loads along the two transverse directions. Core manufacturers therefore provide shear moduli in the 'ribbon' (along the length of a sheet) and 'warp' (along the stack width direction) orientations. Cores are specified by their material, surface density (usually in lb/ft^3, or 'pcf'), and cell size (typically 1/16" to 1").

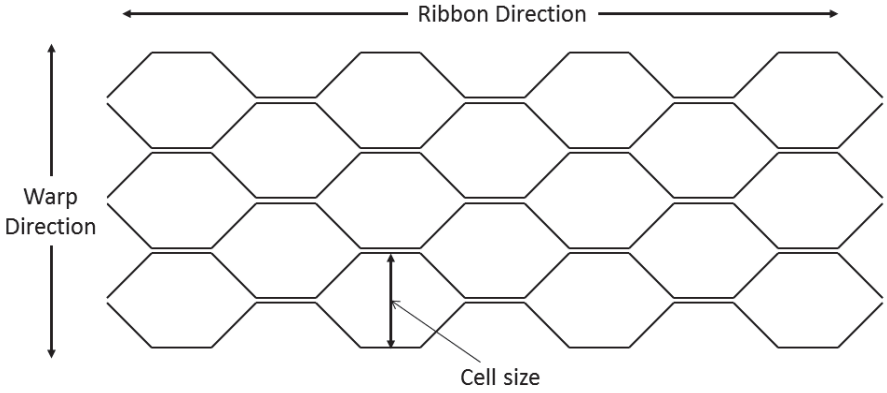

Figure 3. Honeycomb core.

The launch vehicle panel has a Hexcel HexWeb core, CR III 5052 Hexagonal Aluminum honeycomb, 1/8" cell size, 8.1 pcf. The face sheets are made from 8 layers of Carbon plain weave fabric embedded with epoxy with the stackup [0/45/0/45/45/0/45/0]. The numbers in the stackup specification are angles of the fibers in the fabric. Since the fabric is a plain weave, it has fibers oriented in orthogonal directions, such that '0' implies fibers in both the 0 and 90 degree directions. The center two layers are both oriented at 45 degrees, such that the face sheet is symmetric about its center. The roof panel has a Hexcel Hexagonal Kevlar honeycomb, also 1/8" cell size, but lighter at 3.3 pcf. The face sheets, like those of the launch vehicle panel, are made of carbon/epoxy plain weave fabric, but with only 3 layers [0/45/0]. Table 1 summarizes the dimensions and properties of the two panels. Note that the free launch vehicle panel is significantly stronger and heavier than the roof panel.

Table 1 – Dimensions and properties of sandwich panels

Panel	Length (m)	Width (m)	Core Thickness (mm)	Single Facesheet Thickness (mm)	Surface mass density (kg/m^2)	Facesheet Young's Modulus (GPa)	Core Shear Moduli, ribbon/warp (MPa)
Launch Vehicle Panel	2.13	1.22	25.4	8 x 0.267= 2.30	11.7	47.6	931 / 372
Rotorcraft Roof Panel	0.914	0.762	12.7	3 x 0.201= 0.601	3.10	57	139 / 68

2.2 Wavespeeds

Given the face sheet and core dimensions and properties, the effective surface mass density (mass/area), flexural and shear rigidities, and therefore the effective bending wavespeed, may be determined from:

$$c_b^2 = \frac{2N}{\mu_s + \sqrt{(\mu_s)^2 + \frac{4\mu_s N^2}{\omega^2 D}}} \tag{1}$$

where $D = \frac{E_{fs} t_{fs} (h_{core} + t_{fs})^2}{2(1-\upsilon_{fs}^2)}$ is the flexural rigidity, $N = G_{core} h_{core} (1 + t_{fs} / h_{core})^2$ is the shear rigidity, E_{fs} is the Young's Modulus of the facesheet material, h_{core} is the core thickness, t_{fs} is the facesheet thickness, ν_{fs} is the Poisson's ratio of the face sheets, μ_s is the overall surface mass density of the panel and:

$$G_{core} = \sqrt{G_{ribbon} G_{warp}}\,, \tag{2}$$

where G_{ribbon} and G_{warp} are the core shear moduli across the length and width of the honeycomb core. While it is common to use the mean G_{core} to compute averaged bending wavespeeds, individual wavespeeds in the ribbon and warp directions may be also be computed.

Let's examine these parameters further. The flexural rigidity (D) is dictated by face sheet Young's modulus, thicknesses, and offset distance from the panel neutral axis. Compare the sandwich panel D to that of a solid isotropic homogenous panel:

$$D_{simple\ panel} = \frac{Et^3}{2(1-\upsilon^2)} \tag{3}$$

The difference is the h_{core} term in the sandwich panel equation, which is squared. A modest h_{core} of twice the facesheet thickness increases stiffness by a factor of 9, with a negligible increase in mass (typically less than 5%).

The shear rigidity (N) is dictated by the core shear modulus and thickness. Note the frequency dependence of the last term in the denominator of Equation 1. At very high frequencies, that term tends to 0, and the wavespeed becomes simply the shear wave speed of the core. Finally, note that the surface mass density is simply the sum of all the surface mass densities of both face sheets, the core, and in some cases the adhesive.

The flexural wavespeeds in two typical sandwich panels (not the ones in Figure 1) are shown in Figure 4. At low frequencies, the transverse waves are flexural, and depend solely on the flexural stiffness of the face sheets and the overall panel mass. However, the actual effective waves transition to pure shear in the core at higher frequencies. The speed of sound in air is also shown in the examples. Notice how the effective wavespeed in the example on the left exceeds that of the speed of sound in air at a low frequency (about 500 Hz). When transverse waves become supersonic, they couple extremely well with surrounding acoustic fluids.

This strong sound-structure coupling can lead to strong sound transmission, but also high vibration and alternating stress. Many years ago, some structural-acousticians considered adjusting the sandwich panel properties such that the transition from flexural to shear waves occurs very low in frequency, and tuned the shear wave speeds (by softening the core) such that they were subsonic. The right example in Figure 4 shows the wavespeeds for a soft core panel. While intriguing, structural integrity constraints rarely allow such panels to be used in practice.

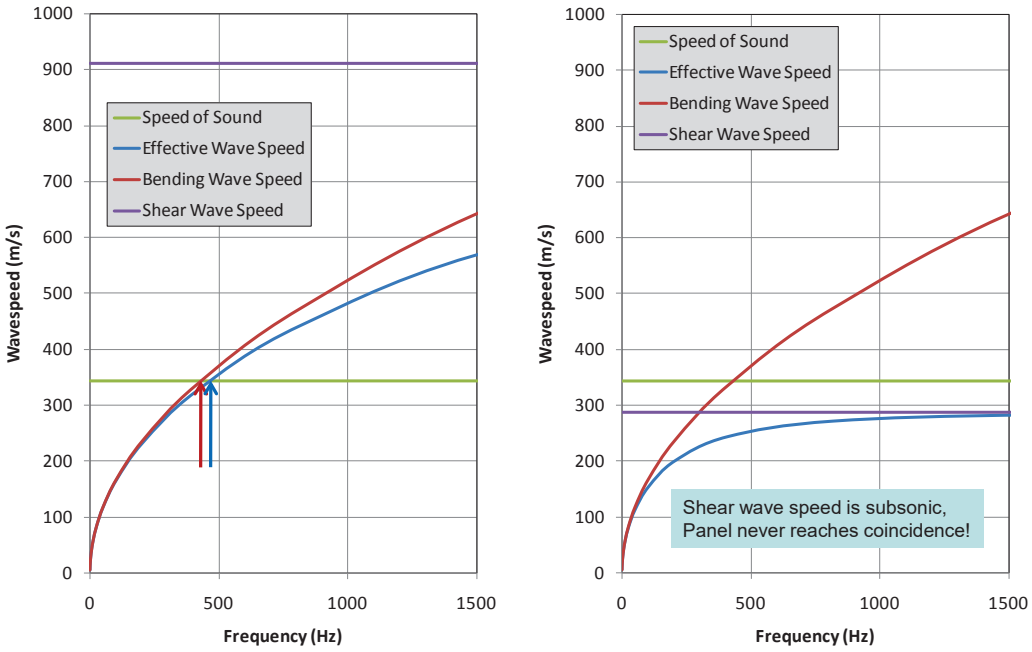

Figure 4. Typical sandwich panel wavespeeds:

Left – panel with high core shear moduli; Right – panel with very low core shear moduli.

2.3 Modes of Vibration

Mode shapes, frequencies, and loss factors of both panels were measured using experimental modal analysis [11]. The modes of the roof panel were also simulated using finite element (FE) analysis of a model constructed with quadratic solid elements Figure 5 shows examples of mode shapes for both panels. Note that the roof panel shapes shown are actually from an FE model so that the frame structure may be visualized.

The mode shapes are classified by mode orders (m, n), where m indicates the mode order along the length, and n indicates the mode order along the width. The mode orders are determined differently for free and simply supported boundary conditions. For free boundaries, count the number of node lines (regions of near zero motion) to compute mode order. For example, the (2,1) launch vehicle panel mode has two node lines along the length, and one node line along the width. For simple supports, count the number of antinodes (regions of maximum motion). For the (3,1) roof panel mode, there are three antinodes along the length, and one along the width.

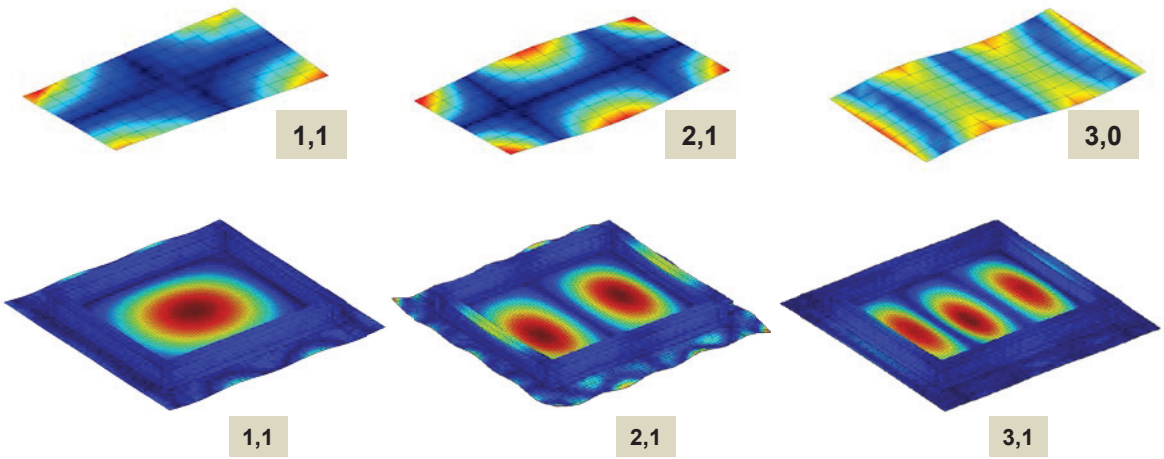

Figure 5. Typical flexural mode shapes:

Top – launch vehicle panel with free boundaries; Bottom – roof panel with simply supported boundaries (note that the frame and outer edging is also shown).

The mode orders, along with the resonance frequencies, may be used to confirm the wavespeed estimates made using the panel properties. Modal wavenumbers for panels with free boundaries may be calculated using:

$$k_m = \frac{\pi(2m-1)}{2a}, k_n = \frac{\pi(2n-1)}{2b} \tag{4}$$

where a and b are the length and width of the panels. For simple supports:

$$k_m = \frac{m\pi}{a}, k_n = \frac{n\pi}{b} \tag{5}$$

For any mode shape, the wavenumber magnitude is:

$$k_{mn} = \sqrt{k_m^2 + k_n^2} \tag{6}$$

Once the wavenumber magnitude is known, the flexural sound speed of a mode at its resonance frequency is simply

$$c_b(m,n) = \omega_{mn} / k_{mn}. \tag{7}$$

Now, the modal wavespeeds may be tabulated and compared to the analytically calculated wavespeeds from Equation (1). The mode orders, resonance frequencies, modal wavenumbers and modal wavespeeds of the launch vehicle panel are listed in Table 2, and compared in Figure 6 to analytic wavespeeds computed using the core shear modulus (warp direction) along the length of the panel. The n=0 modes align well with the analytic estimates, since those modes have no deformation along the width. The other mode orders deform along the width, which aligns with the stiffer (ribbon) direction of the core. These modes therefore have faster wavespeeds.

Figure 7 shows the analytic and modal wavespeeds for the simply supported roof panel. This time, two wavespeed calculations are shown – using the ribbon and warp core shear moduli. The plotted modal wavespeeds are limited to m=1 and n=1 mode orders, so that the modes are aligned as closely as possible along the length and width. The lengthwise (n=1) modes agree very well with the analytic estimates, but the widthwise (m=1) modes are stiffer. This means that the boundary conditions deviate somewhat from the ideal simple supports assumed for the modal wavenumber calculation.

Table 2 – Resonance frequencies, modal wavenumbers, and modal wavespeeds of launch vehicle panel with free boundary conditions

m	n	Freq (Hz)	km (1/m)	kn (1/m)	kmn (1/m)	cb (m/s)
2	0	46	2.21	0.00	2.21	130
3	0	128	3.68	0.00	3.68	218
4	0	255	5.15	0.00	5.15	310
5	0	413	6.63	0.00	6.63	391
1	1	42	0.74	1.29	1.48	176
2	1	99	2.21	1.29	2.56	244
3	1	186	3.68	1.29	3.90	300
4	1	306	5.15	1.29	5.31	362
0	2	162	0.00	3.87	3.87	263
1	2	186	0.74	3.87	3.93	297
2	2	239	2.21	3.87	4.45	337
3	2	331	3.68	3.87	5.34	390
0	3	431	0.00	6.44	6.44	420
2	3	503	2.21	6.44	6.81	464

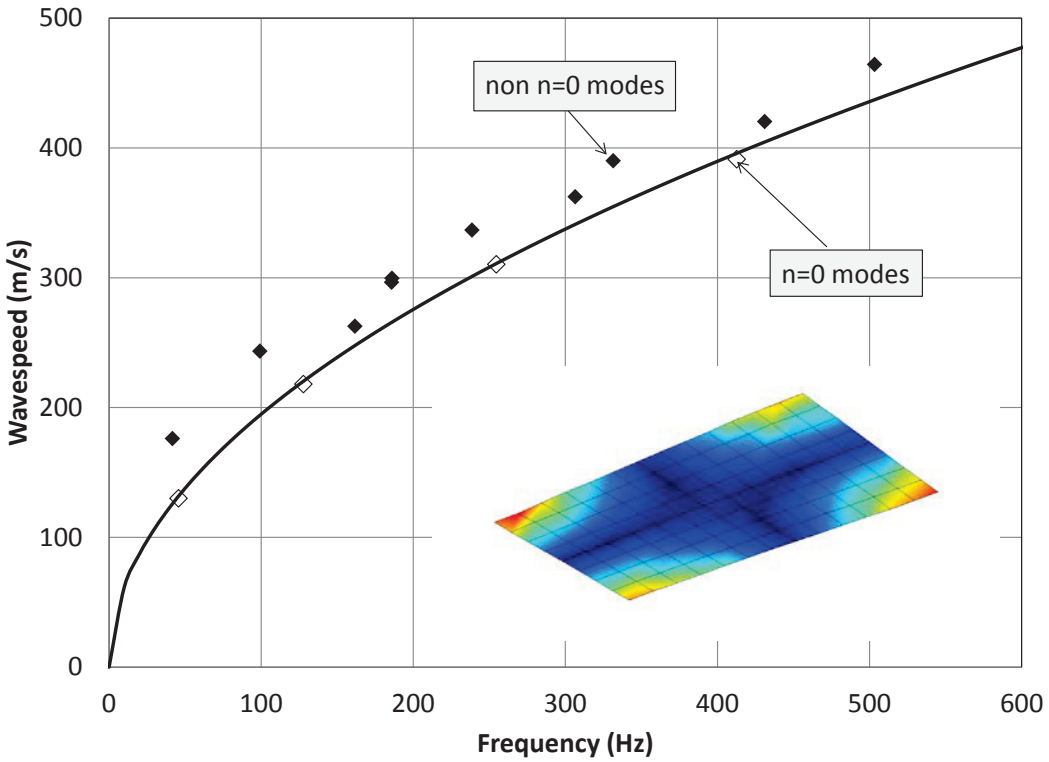

Figure 6. Wavespeeds and modal frequencies of a sandwich panel with free boundary conditions.

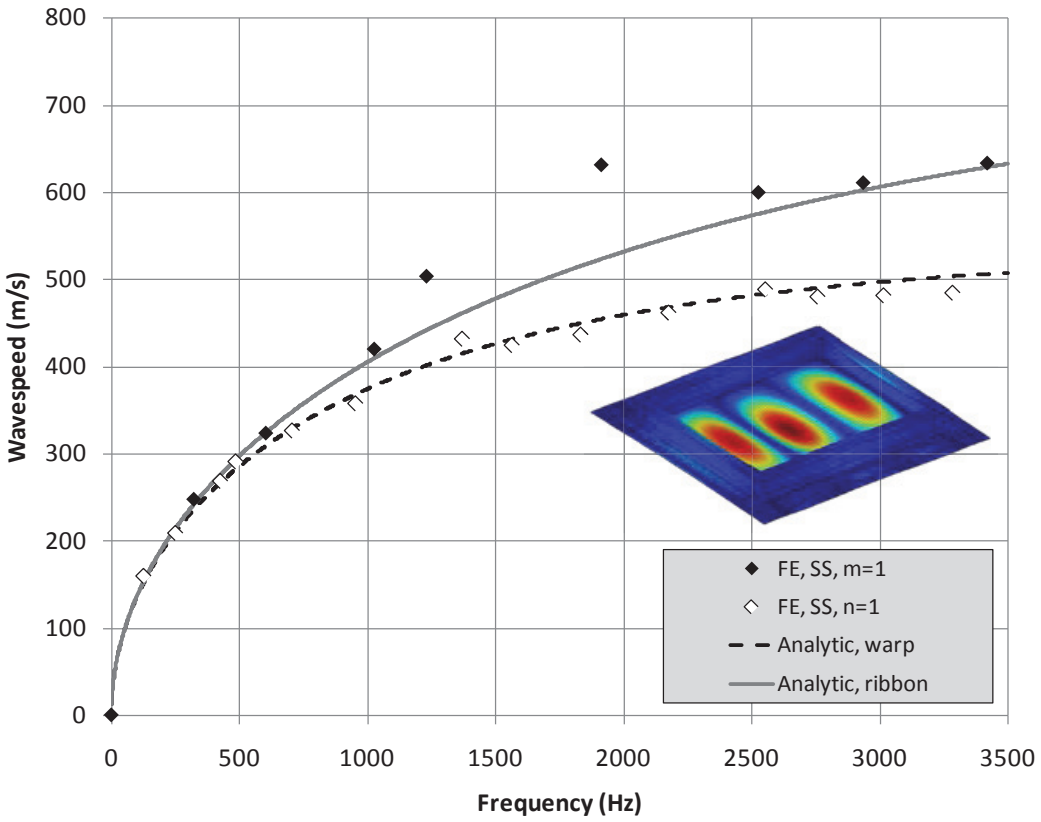

Figure 7. Wavespeeds and modal frequencies of a (nearly) simply supported sandwich panel.

3. RADIATION RESISTANCE AND DAMPING

Modal loss factors were also measured for both panels. The loss factors for the launch vehicle panel are plotted in Figure 8, and show a strong peak between 400 and 600 Hz. The elevated loss factors are caused by sound radiation damping of the panel vibration. Referring to Figure 6, the flexural wave speed coincides with the acoustic wave speed c_o of 344 m/s at about 350 Hz (this is very low compared to the coincidence frequencies of typical metal panels). The critical (lowest coincidence) frequency may be computed directly by setting equation 1 equal to the square of the acoustic sound speed and solving for ω:

$$\omega_{cr}^2 = \frac{c_o^4 \mu_s}{D} \frac{1}{1 - \frac{c_o^2 \mu_s}{N}}. \tag{8}$$

An acoustic boundary element model was coupled to the measured mode shapes of the free launch vehicle panel to compute radiation loss factors [13], which are also plotted in Figure 8. The radiation loss factors clearly dominate the panel loss factors for frequencies up to 1 kHz. Above 1 kHz, the radiation loss factors diminish, so that the panel loss factors are due solely to internal structural damping at high frequencies, which is about 0.007 over all frequencies.

The measured modal damping loss factors of the simply supported roof panel are shown in Figure 9. Once again, the loss factors are highest at low frequencies, and diminish with increasing frequency. Examining Figure 7 reveals that the coincidence frequency is near 600 Hz (slightly higher than that of the launch vehicle panel). Instead of computing radiation damping using acoustic BE analysis, a simple analytic estimate is used instead. Assuming a radiation efficiency of unity, the radiation loss factor is:

$$\eta_{rad_{high}} = \frac{\rho_o c_o}{\omega \mu_s}. \tag{9}$$

The analytic estimate is also plotted in Figure 9, and overestimates the measured modal loss factors. This implies that the structural modal masses are higher than estimated. Examining the mode shapes in Figure 5 reveals that the panel modes are coupled to the beam frame, and in some cases to the external panel edging. The structural mass is therefore increased by 50% and the radiation damping recomputed. The added mass reduces the radiation loss factor so that it is comparable to the observed damping for many (but not all) of the mode shapes. This means that the less damped mode shapes have even higher modal masses due to coupling with the rest of the structure, and that the structural motion of the frame and edging do not couple as strongly with the surrounding air, reducing radiation damping of the overall structure.

4. MOBILITIES

The surface averaged mobilities (normal velocity/applied force) of the launch vehicle panel were measured with impedance heads driven by a shaker, and by accelerometers and impact hammer forces, at six randomly spaced locations. The mobility of an infinite sandwich panel is

$$G_{\text{inf}} = \frac{\omega}{4 \mu_s c_b^2} \left(1 - \frac{1}{2} \left(\frac{c_b}{c_{b_{fs}}} \right)^3 \right) \tag{10}$$

where c_{bfs} is the flexural wavespeed of the face sheets only (based on D in Eq. 3). This is actually a conductance (real part of mobility) since infinite panels have no reactive mobility. The two measured conductances are compared to the analytic conductance in Figure 10. The two measurements align well, and the analytic infinite panel estimate tracks the mean of the measurements, as expected. As the transverse waves transition to pure shear waves, the conductance increases with frequency.

Surface averaged mobilities were also measured for the roof panel using an array of accelerometers and an impact hammer, and were averaged over the accelerometer locations. A numerical FE/BE model was also constructed, and exercised to simulate mobilities, also shown in Figure 11. The acoustic BE model was included in the calculations to include the strong effects of radiation damping. Without adding the damping calculated by the BE modeling to the structural FE model, the simulated mobilities are much higher than those measured. Infinite panel conductances are also compared to the measurements and simulations, computed using the ribbon and warp core shear moduli. The spread of the analytic mobilities envelopes the measured and simulated data well.

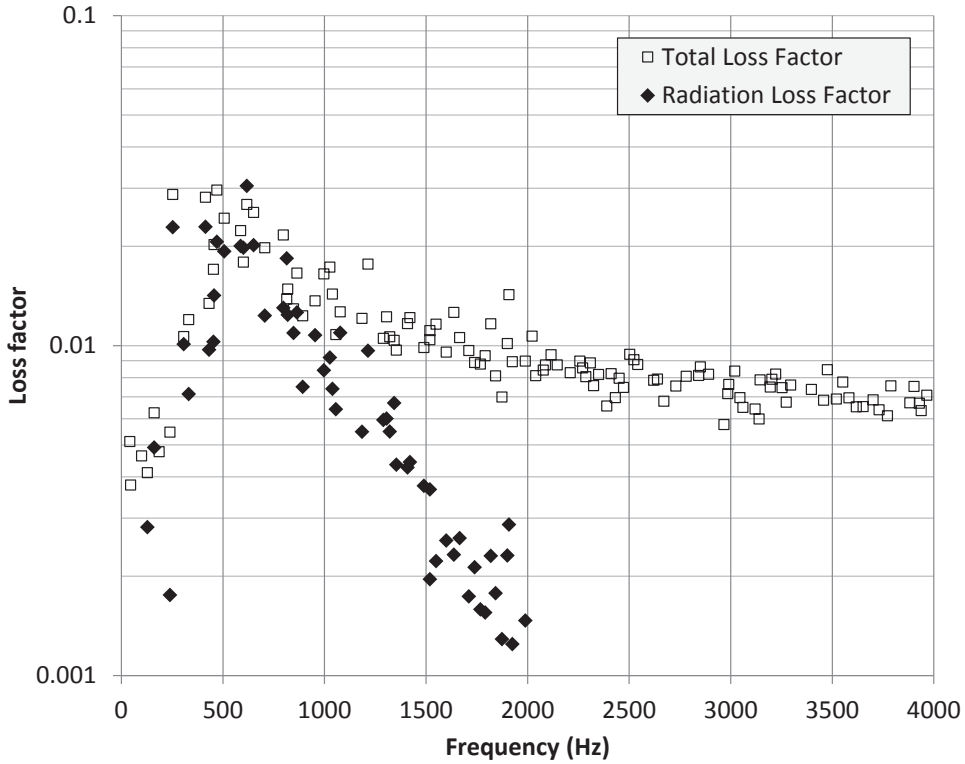

Figure 8. Total measured and calculated (BE) radiation loss factors of launch vehicle sandwich panel.

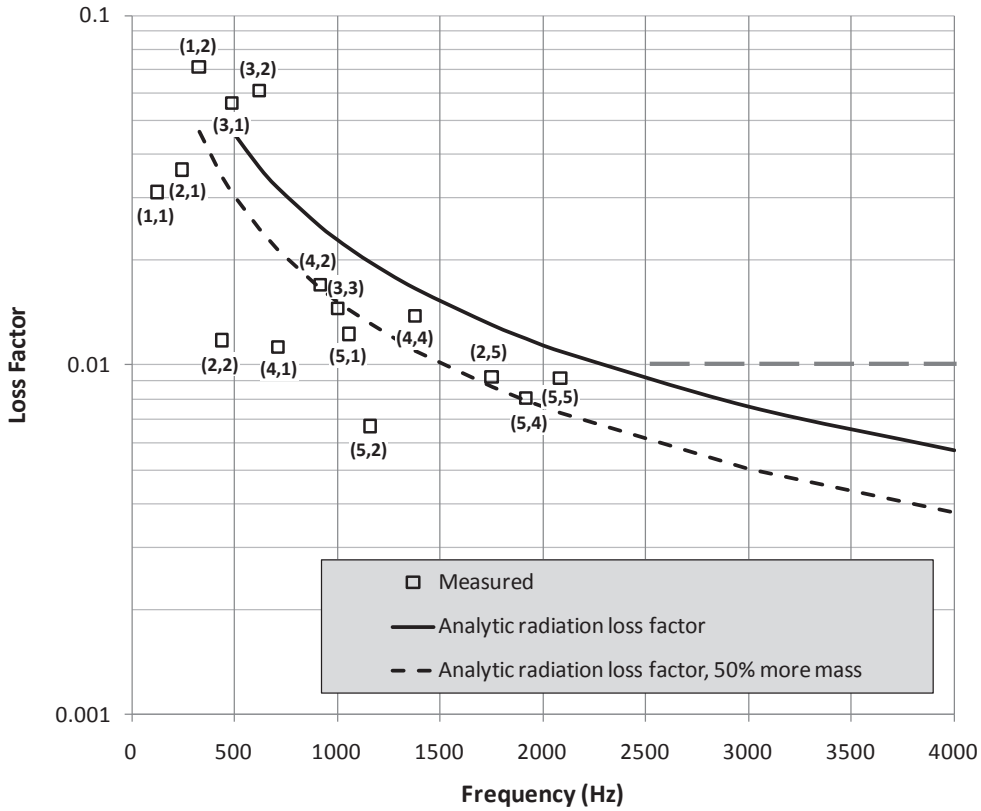

Figure 9. Total measured and analytically estimated radiation loss factors of framed rotorcraft roof sandwich panel.

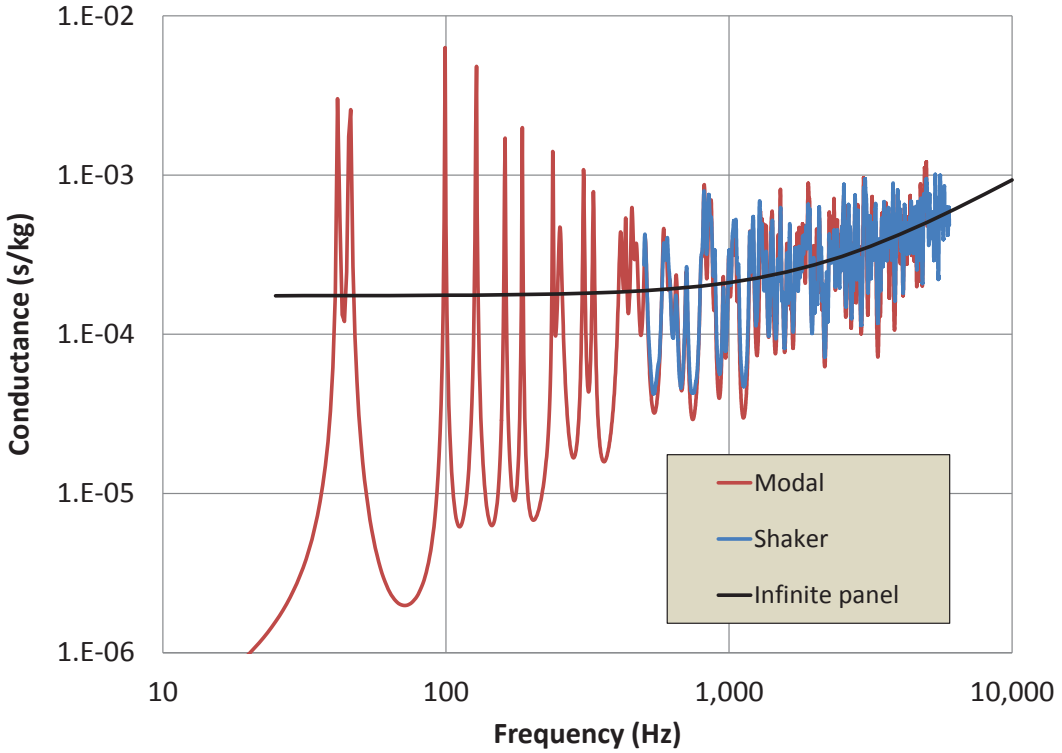

Figure 10. Measured and analytic conductance (real part of mobility) of the launch vehicle sandwich panel.

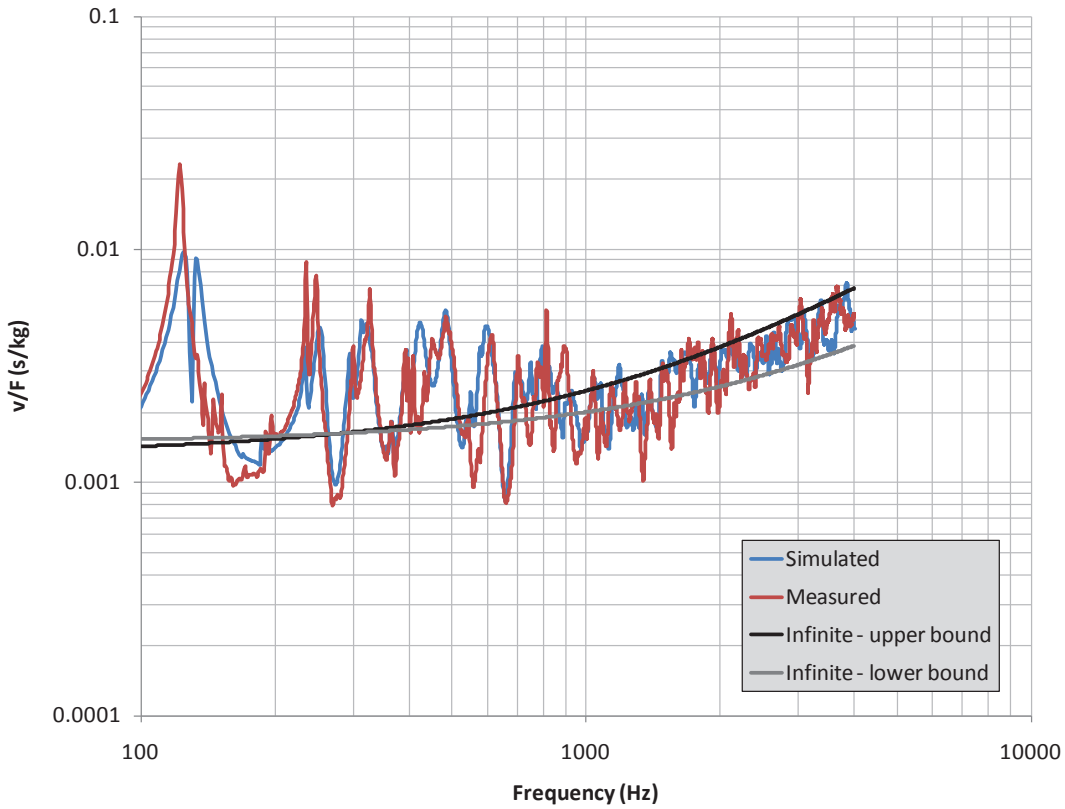

Figure 11. Measured, analytic, and simulated averaged mobilities of the framed rotorcraft roof sandwich panel.

5. SUMMARY AND CONCLUSIONS

In this paper, I have summarized the general vibroacoustic behavior of flexural waves in composite sandwich panels, including how panels are constructed, their wavespeeds and flexural modes, radiation damping, and mobilities. The two examples – a strong launch vehicle panel with free boundaries and a framed rotorcraft roof panel with approximately simple supports – show similar behavior: low acoustic coincidence frequencies and high radiation damping, and a transition to pure shear waves at low frequencies. The sandwich panel flexural wave speed formula is confirmed using modal wavespeeds, and the effects of differing core shear moduli in the ribbon and warp directions are evident in the measured data. Radiation damping may be estimated simply using an assumed radiation efficiency of unity, or rigorously with acoustic BE modeling. Radiation damping must be included in any FE simulation of mobility.

ACKNOWLEDGEMENTS

I am grateful to my co-authors of the previous papers and reports on sandwich panels cited in the reference section, including Drs. Stephen Conlon, Micah Shepherd, Rob Campbell, John Fahnline, and Andrew Barnard.

REFERENCES

1. Hambric, S.A., “Structural Acoustics Tutorial – Part 1: Vibrations in Structures,” *Acoustics Today*, Vol. 2, Issue 4, October 2006.
2. Hambric, S.A., “Structural Acoustics Tutorial – Part 2: Sound-Structure Interaction,” *Acoustics Today*, Vol. 3, Issue 2, April 2007.
3. Hambric, S.A., “Tutorial on infinite panel sound transmission loss simulations,” *Proceedings of Internoise 2015*, San Francisco, CA, USA, 9-12 August 2015.
4. Hambric, S.A., Conlon, S.C., Grisso, B.G., and Shepherd, M.R., “Measurements of the Power Flow Between Bolted Honeycomb Sandwich Panels,” *Proceedings of Internoise 2009*, Ottawa, Canada, August 2009.
5. Hambric, S.A., Barnard, A.R., and Conlon, S.C., “Power transmission coefficients based on wavenumber processing of experimental modal analysis data for bolted honeycomb sandwich panels,” *Proceedings of Internoise 2010*, Lisbon, Portugal, 13-16 June 2010.
6. Hambric, S.A., et.al., “Experimental vibro-acoustic analysis of honeycomb sandwich panels connected by lap and sleeve joints,” *Proceedings of Internoise 2011*, Osaka, Japan, 4-7 September 2011.
7. Hambric, S.A., Shepherd, M.R., May, C., and Snider, R., “Vibro-acoustic measurements and simulations of a rib-framed honeycomb core sandwich panel,” *Proceedings of Internoise 2013*, Innsbruck, Austria, 15-18 September 2013.
8. Hambric, S.A., Shepherd, M.R., Snider, R., and May, C., “Quieting a rib-framed honeycomb core sandwich panel for a rotorcraft roof,” *Proceedings of Internoise 2014*, Melbourne, Australia, 16-19 November 2014.
9. Hambric, S.A., and Shepherd, M.R., “Measurements of the air-borne and structure-borne sound power transmission through a quiet honeycomb core sandwich panel for a rotorcraft roof,” *Proceedings of Internoise 2015*, San Francisco, CA, USA, 9-12 August 2015.
10. Hambric, S.A., Shepherd, M.R., Koudela, K., Wess, D., Snider, R., May, C., Kendrick, P., and Lee, E., *Acoustically Tailored Composite Rotorcraft Panels*, *NASA/CR-2015-218769*, July 2015.
11. Hambric, S.A., Fahnline, J.B., Campbell, R.L., Shepherd, M.R., and Conlon, S.C., “Modal based experimental vibro-acoustic analysis of sandwich panels,” *Proceedings of NOVEM 2015*, Dubrovnik, Croatia, 13-15 April 2015.
12. Hambric, S.A., Sung, S.H., and Nefske, D.J. (editors), *Engineering Vibroacoustic Analysis: Methods and Applications*, Wiley, 2016.
13. Shepherd, M.R., Fahnline, J.B., Dare, T.P., Hambric, S.A., and Campbell, R.L., " A hybrid approach for simulating fluid loading effects on structures using experimental modal analysis and the boundary element method," *Journal of the Acoustical Society of America*, 138 (5), 3073-3078, November 2015.